Processing of binary fringe patterns obtained by phase-shifting time-averaged shearography on vibrating objects

Murielle Kirkove[1,*], Stéphanie Guérit[2,*], Laurent Jacques[2], Jean-François Vandenrijt[1], Fabian Languy[1], Christophe Loffet[3], Marc Georges[1]

[1]Centre Spatial de Liège—Université de Liège, Liege Science Park, B-4031 Angleur, Belgium

[2]Institute of Information and Communication Technologies, Electronics and Applied Mathematics (ICTEAM) - Université catholique de Louvain (UCL), B-1348 Louvain-la-Neuve, Belgium

[3]V2i S. A., Liege Science Park, B-4031 Angleur (Liège), Belgium

ABSTRACT

Shearography can be used for full-field strain measurements in the field of vibration analysis. It provides the spatial derivative of the optical phase difference of the vibration modes amplitude along the so-called shear direction. The shearographic setup considered here is based on the phase-shifting time-averaged technique. It can easily be applied experimentally, but its drawback is that binary phase patterns are obtained. These phase changes are related to the zeroes of a Bessel function. Retrieving the corresponding displacement maps is not straightforward. Moreover, integration of shearographic results need to be performed, and this step is sensitive to noise in the patterns. In this paper, different processing stages are described, from fringe denoising to integration of the displacement maps. The application on data acquired in industrial environment illustrates the good performances of the proposed method.

1. INTRODUCTION

Electronic speckle pattern interferometry (ESPI) [1] and speckle shearing interferometry (shearography) [2] are two contactless optical techniques used in the field of non-destructive testing and vibration analysis [3]. Vibration phenomena can be studied in terms of amplitude, speed and acceleration. ESPI and shearographic techniques provide measurement related to the amplitudes of vibrations.

Shearography records the interference pattern between a speckle object wavefront and itself laterally displaced through an optical shearing device [2]. Such interference (fringes) patterns, so-called shearograms, are recorded at different instants of the vibration test. The numerical difference between two shearograms gives rise to an interferogram that allows observing the derivative of the full-field displacement of the object along the optical shear direction. Shearography is less sensitive to environmental disturbances than ESPI and, when applied with visible lasers, it is the only technique among the both which is able to cope with highly unstable environments. It has hence become an important measurement tool outside the optics laboratory [3][4].

In the case of vibration measurement, like all other interferometry techniques, shearography has been demonstrated through various methods. The best-known is the time-averaging (TA) in which shearograms are recorded over an integration time much longer than the object vibration period. Assuming the object is sinusoidally excited, the intensity images show Bessel-type interference fringes with a maximum of intensity at the vibration nodes and a rapidly decreasing contrast from the nodes to antinodes [5][6]. As Bessel fringes are generally difficult to interpret automatically, one may prefer alternative methods. One of them is the stroboscopic real-time method [6][7], but the latter requires additional device for stroboscopic operations. An interesting alternative combines the basic TA technique with the phase-stepping [9][10]. The resulting phase-stepped time-averaged (PSTA) method [11] is easy to implement since a basic interferometric (i.e. not specifically developed for vibrations) can be used. However, this method provides binary phase fringes which cannot be unwrapped for subsequent displacement map computation. However, they are far sufficient for identification of mode shapes, e.g. through comparison with calculated ones. We already presented developments and application of PSTA shearography for mode shapes visualization in industrial environments. [12][13].

In this paper we propose a post-processing method going one step further, in view of qualitative assessment of vibration amplitudes from PSTA shearography. The method is divided into two stages: pre-processing and processing. Pre-processing attenuates the noise contained in the acquisitions while processing stage reconstructs the displacement and vibration amplitude maps. The processing is divided into three steps. The first one delineates the fringes in the pre-processed image. The second one estimates the displacement map as a piecewise constant function with these fringes as sub-domains. Finally, the last step provides vibration amplitude maps by integration of the displacement maps. Denoising is a critical part of the method since, combined with the first processing step, it helps to better identify the fringes in the shearographic measurements. We present a qualitative evaluation of the processing from real data.

The paper is structured as follows. Section 2 reviews the basics of PSTA shearography method and describes the two experimental data sets which are subsequently used. Section 3 describes the pre-processing steps to apply on data prior to the main processing. In section 4, we describe the processing steps, finishing with integration, and the results on real data.

2. BASICS OF THE PSTA SHEAROGRAPHY METHOD

2.1. Description of setup

As illustrated in Fig. 1, shearography acquisition proceeds by illuminating an object under vibration with a laser. Light scattered by the object surface is observed by a camera through a shearing device of Michelson interferometer type. The latter consists of a beam-splitter cube (BS) with mirrors M_1 and M_2 placed in the transmitted and reflected arms of the BS respectively. This assembly splits the object image into two parts that are retro-reflected by two mirrors before entering a camera with its objective lens (OL).

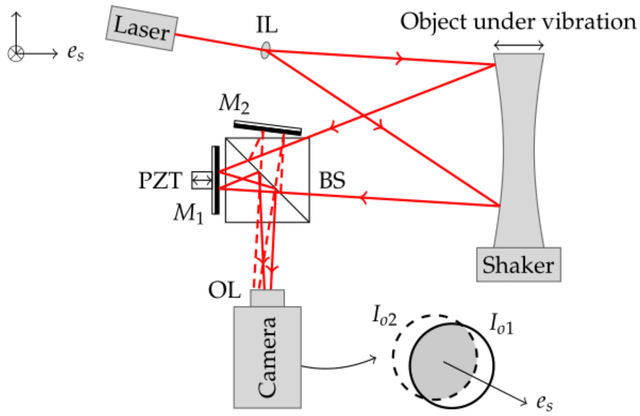

Fig. 1 Shearography setup and resulting shifted images with overlap in gray.

If one of the mirrors is slightly tilted (e.g., M_2 in Fig. 1), both reflected images I_{o1} and I_{o2} appear transversally shifted from another in the direction es. The shift is called the shear displacement and the direction es the shear direction. In the overlapping region (see gray area in Fig. 1), interference occurs, giving rise to the so-called shearogram.

During vibration, the instantaneous intensity in each pixel of the camera plane is given by

$$\begin{cases} I_{inst}(t) = I_{o1} + I_{o2} + I_m cos(\phi + \delta(t)) \\ I_m = 2(I_{o1} I_{o2})^{1/2} \end{cases} . \tag{1}$$

Where I_m is the modulation intensity, ϕ is the phase difference between both interfering images and δ is the optical phase variation due to vibration displacement, which is given by

$$\delta(t) = \delta_A \sin(\omega t). \tag{2}$$

with δ_A, the amplitude of the optical phase variation, and ω is the cyclic frequency of vibration. Our method assumes time-averaging of the instantaneous intensity profile given by (1) obtained by recording shearograms over a time longer than the period of vibration $2\pi/\omega$. The resulting pattern can be described as [13]

$$I = I_{o1} + I_{o2} + I_m cos(\phi) J_0(\delta_A), \tag{3}$$

where J_0 is the 0th order Bessel function of first kind.

At any time, the phase difference $\Delta\phi$ between the phase ϕ and a reference phase ϕ_r, related to the resting state (i.e., without vibration), can be computed using the phase-shifting technique [14]. This consists in acquiring a set of shearograms with an additional known phase shift between each capture. For that purpose, a piezoelectric translator (PZT) moves mirror M1 to produce the phase shift (see Fig. 1). Usually we use the 4-steps algorithm with a phase shift $\Delta\phi_s$ of $\pi/2$. The four acquisitions are expressed as

$$I_k = I_{o1} + I_{o2} + I_m \cos(\phi + k\Delta\phi_s) J_0(\delta_A), \tag{4}$$

for $k \in \{0,1,2,3\}$. At rest, δ_A is 0 so that $J_0(\delta_A)$ is 1 (see Fig. 2) and ϕ_r is computed from the four acquisitions [1] by

$$\phi_r = \tan^{-1}\left(\frac{I_3 - I_1}{I_0 - I_2}\right). \tag{5}$$

When vibration occurs, $J_0(\delta_A)$, the multiplicative term in Eq. (4), takes any real value. Phase ϕ is undefined when $J_0(\delta_A)$, is 0 and, otherwise, is computed on each pixel by

$$\phi = \tan^{-1}\left(\frac{I_3 - I_1}{I_0 - I_2}\right) + \begin{cases} 0 \text{ if } J_0(\delta_A) > 0 \\ \pi \text{ if } J_0(\delta_A) < 0 \end{cases}. \tag{6}$$

Combining Eq. (5) and Eq. (6), the difference $\Delta\phi$ is

$$\Delta\phi = \begin{cases} 0 & \text{if } J_0(\delta_A) > 0 \\ \pi & \text{if } J_0(\delta_A) < 0 \\ \text{undefined} & \text{otherwise} \end{cases}. \tag{7}$$

Fig. 2 illustrates the variation of $\Delta\phi$ with respect to $\overline{\delta_A}$, the absolute value of δ_A. Eq. (7) shows that PSTA shearography only provides a binary phase pattern $\Delta\phi$ which is related to amplitude of optical phase variation δ_A. The purpose of the current paper is to propose a method that estimates the map of vibration amplitudes φ_A. (i.e. the vibration mode shape), related to δ_A through the following formula [2]

$$\delta_A = \frac{4\pi}{\lambda}\frac{\partial\varphi}{\partial s}\Delta_s, \tag{8}$$

where $\frac{\partial}{\partial s}$ is the directional derivative in the shear direction es and Δ_s, is the shear displacement.

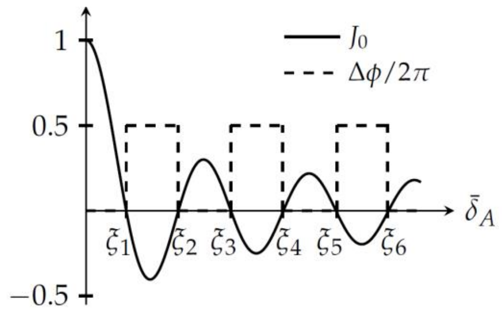

Fig. 2 Variation of phase differences $\Delta\phi$ with respect to the absolute values of directional displacements of vibration amplitudes in the shear direction ($\overline{\delta_A}$). The first six zeros ξ_k (k=1, …, 6) of the Bessel function J_0 are shown.

2.2. Description of experimental data

We acquired shearographic measurements of a metallic turbine blade under vibration. First, the so-called optics laboratory data have been obtained in very stable conditions in laboratory. They correspond to the left frame of Fig. 3. The blade base was clamped in a dedicated support attached to the stud of a shaker used to test the blade under vibration.

The blade size ($5\times4cm^2$) is representative of the object sizes investigated in industrial environment. The shaker allows vibrations up to a few tens of kHz. The setup includes a continuous diode pumped laser at 532 nm wavelength (from company Coherent, model Verdi) and a CCD camera (from company Allied Vision, model Manta G 145) [12], [13]. The final image size is 686×756 pixels out of the 1388×1038 available ones. Left frame of Fig. 3 shows the binary phase patterns $\Delta\phi$ acquired by shearography at resonance frequencies of 2910, 7960, 8450, and 8630 Hz, corresponding respectively to columns 1, 2, 3, and 4. The rows (a), (b), and (c) correspond to shear directions respectively vertical, horizontal, and diagonal, all with a shear amount of 1 mm.

A second series of data have been acquired in industrial conditions, with shakers of V2i Company. They correspond to images displayed in the right frame of Fig. 3. The equipment is the same as for the optics laboratory experiment, except that the laser which is a LMX from Oxxius manufacturer, emitting 300 mW at 532 nm. Also we used a band-pass filter centered at that wavelength for rejecting spurious ambient light (laser line cleanup filter from manufacturer Edmund). The blade is about 5×10 cm^2 in size and occupies a small region in the field of view, with a final image of 400×800 pixels or 430×450 pixels (depending on the vibration setting) out of the 1280×1024 available ones. The shaker allows vibrations up to a few kHz and the frequencies of the acquisitions are in the range [360, 1250] Hz. This dataset permits testing the method in a range of frequencies lower than the one of optics laboratory. Actually, both datasets cover the resonance frequencies between about 0.1 and 10 kHz. Right frame of Fig. 3 shows images of phase differences acquired by shearography at various resonance frequencies and shear settings.

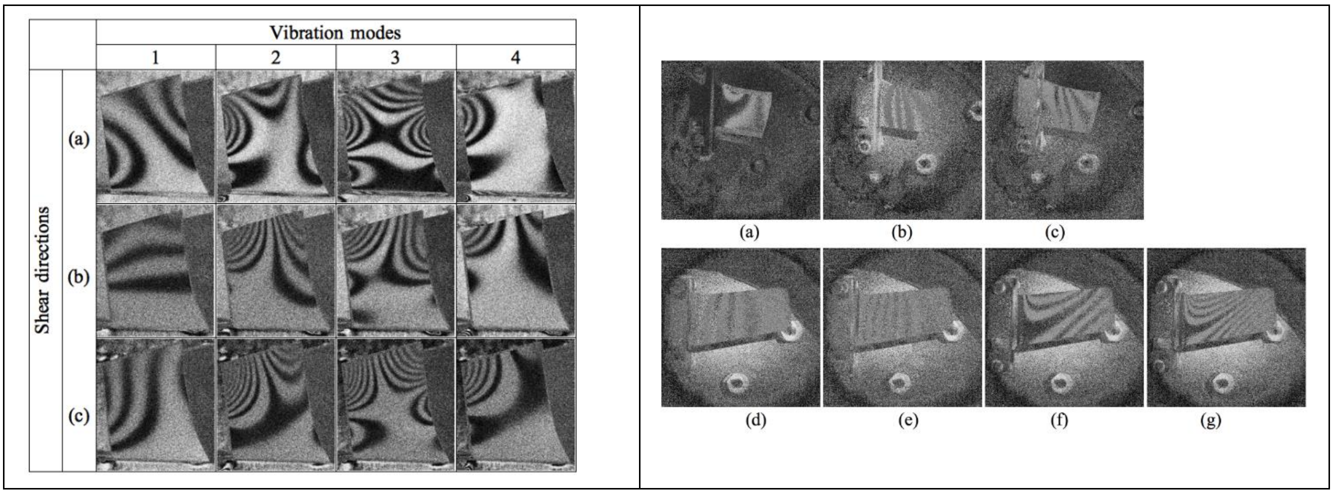

Fig. 3 Images of phase differences acquired by PSTA shearography. (left frame) Patterns obtained at 4 resonance frequencies up to 10 kHz and for 3 shear directions. (right frame) Patterns obtained at various resonance frequencies and shear settings. The frequencies are in the range [360, 1350] Hz. The shear amplitude is 5 mm in vertical (a) and horizontal (b-g) directions.

3. PRE-PROCESSING STEPS

The method we propose for estimating the map of vibration amplitudes from shearographic measurements is based on accurate delineation of the fringes in the original acquisition. Like other interferometric techniques, shearography is subject to high levels of noise (see in particular Fig. 3 (right frame)). Therefore, pre-processing is required for attenuating the noise contained in the original observations. Also another phenomenon can be seen in some figures of Fig. 3, in particular those obtained in industrial conditions. Instead of having well defined phase 0 or π (black or white, like in Fig. 3), we have sometimes of constant phase added, so we can have light grey and dark grey fringes. This does not help to observe clearly qualitatively the mode shape. This is probably related to bad application of phase-stepping in industrial environment. Therefore, phase rotation will be needed too. In the following subsections, we will present the principle of phase rotation and denoising,

3.1 Phase rotation and denoising

From now, we work in a discrete framework. The two-dimensional images of size $n_1 \times n_2$ are vectorized and belong to $\mathbb{R}^N$ where $N = n_1 n_2$. Pixel intensities of images are in [0, 2π[. We denote the 2π-modulo operator by $\mathcal{M}_{2\pi}$. Let $\Delta\phi \in \mathbb{R}^N$ be the measurand, i.e. the original image of phase differences. We only have access to observations $z \in \mathbb{R}^N$, a wrapped and noisy version of $\Delta\phi$, which can be expressed as follows

$$z = \mathcal{M}_{2\pi}(\Delta\phi + n), \quad (9)$$

where $\Delta\phi$ can only take values in $\{\Delta\phi_0, \Delta\phi_{0+\pi}\}$ (see Eq. (7)) and $n \in \mathbb{R}^N$ is an additive Gaussian noise where each n follows a Gaussian distribution of 0 mean and variance σ_n^2.

Pre-processing looks for a good estimate $\Delta\phi_p$ for $\Delta\phi$ based on observations z. This stage is divided into two steps: phase rotation and denoising. We consider two denoising techniques. The first one is an adaptation of the well-known median filtering to phase images (MF). The second one is based on the resolution of an inverse problem enforcing the estimate to be piecewise constant, i.e., to have a small total variation (TV) [15].

3.1.1. Phase rotation

Theoretically, the pixel intensities of fringes should only be 0 or π. Translating (or rotating on the circle $[0,2\pi[$) the two peaks of the histogram to π/2 and 3π/2 minimizes the noise outliers resulting from phase wrapping in regions of lower and higher intensities (see right tail of noise distribution in Fig. 4). The histograms of pixel intensities inside the blade (selected with the blade mask M_b) show however initial distributions with two peaks located at $\Delta\phi_0$ and $\Delta\phi_{0+\pi}$. The first step of pre-processing is consequently a phase rotation of the pixel values of z. The following transformation is applied to the data,

$$z_r = \mathcal{M}_{2\pi}(z - \Delta\phi_0 + \pi/2). \quad (10)$$

3.1.2. Denoising with median filter

Principle and implementation. The common way for removing noise in images of phase fringe patterns is applying a sine/cosine average filter [16]. The application of this principle is introduced in our context as follows. Filtering z_r with linear filter such as average or Gaussian filter would smooth the 2π discontinuities due to the wrapping operator. This problem is solved by calculating the sine and the cosine of z_r which leads to the continuous fringe patterns sin zr and cos z_r. These patterns are then individually filtered and the filtered version of z_r is obtained by applying successively the operators $\tan^{-1}$ and $\mathcal{M}_{2\pi}$. Such filtering process is called sine/cosine filtering. For a filter operator F, its application on z_r leads to the estimate $\hat{z}_r$ defined as

$$\hat{z}_r = \mathcal{M}_{2\pi}(\tan^{-1}(F(\sin z_r)/\, F(\cos z_r))). \quad (11)$$

The median filter M_f is a non-linear filter [17]. Its application on z_r is defined at pixel i as

$$\left[M_f(z_r)\right]_i = \text{Median}\{(z_r)_j \middle| j \in W_\alpha(i)\}, \quad (12)$$

where $W_\alpha(i)$ is a square window of width α centered at pixel i. This non-linear filtering is more effective than linear filters for preserving edges and reducing impulse noise [18], [19]. In this paper, we consider a sine/cosine median filter for which the operator F in Eq. (11) is M_f.

3.1.3. Denoising via regularized inverse problem formulation

Filtering is useful to denoise images when only corrupted observations are available. However, extra knowledge about the acquisition model, the smoothness properties of the pure image or the noise statistics allows us to formulate the denoising problem as an inverse problem. Such a problem aims at reversing the corruption process from the observations.

Forward model. A key element in inverse problem resolution is to have an appropriate mathematical expression for the forward model, i.e., the model relating the observations to the original data. In our case, based on the knowledge of the ideal acquisition process (see section 2) and on visual inspection of the histograms of experimental observations, the forward model can be described in first approximation as equation (9). We will work with the equivalent equation for rotated observations defined by Eq. (10)

$$z_r = \mathcal{M}_{2\pi}(\Delta\phi_r + n), \tag{13}$$

where $\Delta\phi_r = (\Delta\phi - \Delta\phi_0 + \pi/2)$ can only take values in {π/2, 3π/2}. Eq. (11) can be approximated as follows:

$$z_r \approx \Delta\phi_r + n + n' \quad \in [0,2\pi[, \tag{14}$$

with an additive noise $n' \in \mathbb{R}^N$ where n_i' is distributed according to the following distribution knowing $(\Delta\phi_r)_i$:

$$n_i' = \begin{cases} 0 & w.p.\ p_0 = \mathbb{P}(-(\Delta\phi_r)_i \le n_i \le 2\pi - (\Delta\phi_r)_i), \\ -2\pi & w.p.\ p_1 = \mathbb{P}(n_i > 2\pi - (\Delta\phi_r)_i), \\ 2\pi & w.p.\ p_2 = \mathbb{P}(n_i < -(\Delta\phi_r)_i), \end{cases} \tag{15}$$

where w.p. means with probability and $\mathbb{P}$ is the probability symbol. In words, the modulo operator is replaced by an impulse noise having the same effect on the data. Probabilities p_0, p_1, and p_2 depend on the variance σ_n^2 and on the values of $\Delta\phi_r$. We are not interested in the exact knowledge of the distribution of n_i' but rather in the shape and decay of this distribution (see Fig. 4 for theoretical distribution $f(n_i + n_i')$).

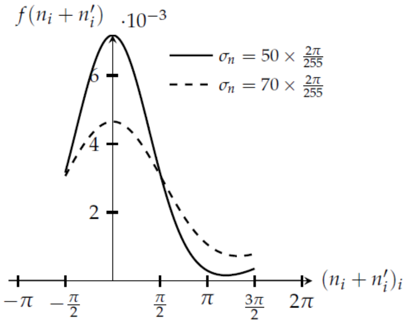

Fig. 4 Theoretical probability density function (pdf) of the additive noise $n_i + n'_i$ on pixel i with intensity $(\Delta\phi_r)_i$ = π/2. The pdf is represented for two different standard deviation σ_n .

Principle. The estimate of the original and noiseless image is computed via the resolution of the following minimization,

$$\Delta\phi_p = \arg\min_{x\in\mathbb{R}^N} \|x - z_r\|_1 + \alpha\Phi(x) \text{ subject to } x \ge 0, \tag{16}$$

where the first and second terms are called data fidelity term and regularization term, respectively. The ℓ_1-norm, noted $\|*\|_1$in Eq.(16), is well adapted for data corrupted by noise with outliers or by impulse noise, namely noise with heavy-tailed distribution [20] [21]. We observe this behavior in shearographic measurements when the noise level is high (see Fig. 4). The regularization term $\Phi(x)$ stabilizes the inverse problem, initially ill-posed, by adding a priori knowledge on $\Delta\phi_p$. Parameter $\alpha > 0$ can be considered as a parameter making the trade-off between the two terms.

In this work, noiseless phase maps are expected to be represented as images with fringes intensities equal to $\pi/2$ or $3\pi/2$ separated by smooth delineation curves. Therefore, the natural regularizing term Φ is the total variation (TV) norm which is minimal for cartoon-like images [15]. Total variation of an image $x \in \mathbb{R}^N$ is defined as the ℓ_1-norm of its gradient magnitude,

$$\Phi_{\mathrm{TV}}(x) = \|\nabla x\|_{2,1} = \textstyle\sum_{i=1}^N \|(\nabla x)_i\|_2 \,. \tag{17}$$

Symbol ∇ represents the discrete gradient operator, defined as

$$\nabla: \mathbb{R}^N \to \mathbb{R}^{2N}, x \mapsto (\nabla x) = (\nabla_1 x^T, \nabla_2 x^T)^T, \tag{18}$$

where $\nabla_i \in \mathbb{R}^{N\times N}$ is the first spatial derivative along direction e_i, approximated numerically by first-order finite differences.

Total variation acts however only locally and can lead to non-smooth fringes delineation (known as staircasing effect). To circumvent this in a future work, we could use a regularization term enforcing sparsity of the image in the curvelet domain [22] or denoise $\mathbb{S}^1$-intensity valued images (with $\mathbb{S}^1$ the periodic circle) instead of estimating the impact of the wrapping operator [23].

Implementation. For numerical implementation, Eq. (16) can be rewritten as an unconstrained minimization problem,

$$\Delta\phi_p = \arg\min_{x\in\mathbb{R}^N} \|x - z_r\|_1 + \alpha\Phi(x) + \imath_{\mathbb{R}_+^N}(x), \tag{19}$$

where indicator function $\iota_{\mathbb{R}_+^N}$ equals to zero if x is non-negative and to $+\infty$ otherwise. Optimal parameter α is such that $\|\Delta\phi_r - z_r\|_1 = \left\|\Delta\phi_p - z_r\right\|_1$, i.e., the ℓ_1-norms of noise and residual after denoising are equal. This optimal value is approximated by $\hat{\alpha}$, a parameter computed iteratively as follows. First, an (under)estimation of the noise ℓ_1-norm $\hat{n}_{\ell_1}$ is computed via fast MF denoising of z_r with a window width equal to 3. We choose large initial value for $\hat{\alpha}$. Estimate $\hat{\alpha}$ is updated after each denoising step according to the following rule:

$$\hat{\alpha}^{(k+1)} = \hat{\alpha}^{(k)}\left(\hat{n}_{\ell_1} / \left\|\Delta\phi_p^{(k)} - z_r\right\|_1\right). \tag{20}$$

This rule is applied only if the multiplicative factor is smaller than 1. Although heuristic, this updating rule allows for an automatic choice of the regularization parameter and gives good results, both for MF and TV denoising. The algorithm used to solve Eq. (19) is the Chambolle-Pock primal dual algorithm [21]. It belongs to the family of proximal algorithms based on the concept of proximal operator [24]. Proximal algorithms are able to solve convex problems with non-smooth and non-differentiable objective function, like Eq. (19).

3.2 Qualitative performance based on real experimental data

Due to the sparsity of experimental results in terms of fringe density and noise levels, we only are able to qualitatively evaluate the denoising techniques by using a visual criterion: their ability to restore distinct fringes.

We pre-processed real data (from optics laboratory and industrial environment) with both denoising techniques. All the experiments were conducted with automatic selection of regularization parameter $\hat{\alpha}$. Fig. 5 show pre-processing results on mode #2 obtained in optics lab. Pre-processing results on the acquisitions from industrial environment with the highest fringes density (corresponding to Fig. 3f and Fig. 3g (right frame)) are illustrated on Fig. 6.

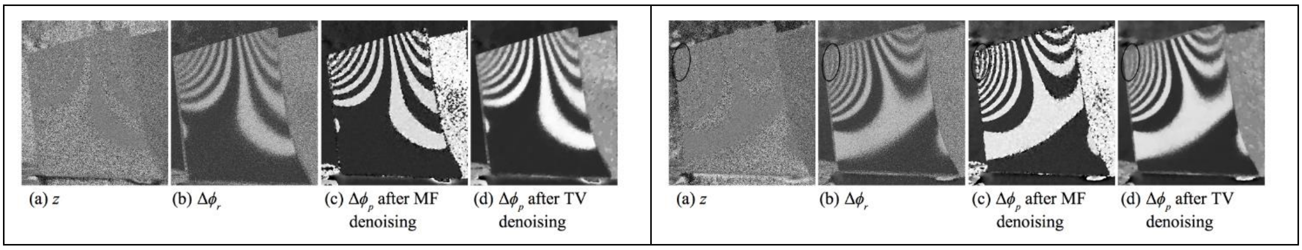

Fig. 5 Pre-processing results for the acquisition at vibration mode 2, (left frame) with horizontal shear direction and (right frame) with diagonal shear direction. Black ellipses indicate areas where identification of fringes is difficult due to high fringes density.

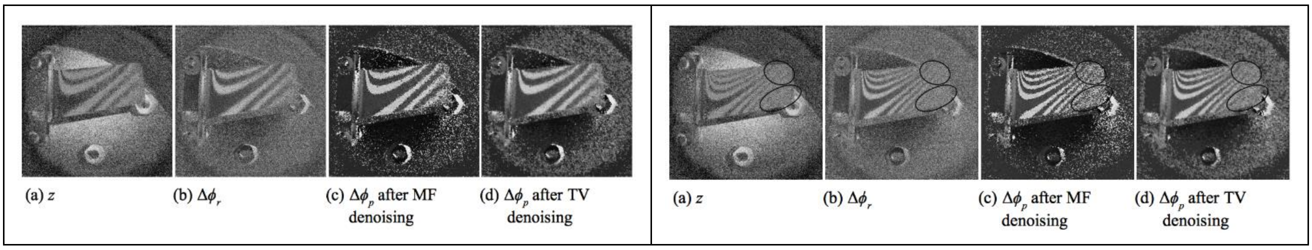

Fig. 6 (Left frame) Pre-processing results for acquisition of Fig. 3f. (Right frame) Pre-processing results for acquisition of Fig. 3g. Black ellipses indicate areas where identification of fringes is difficult due to high fringes density.

Fringe identification is easier after pre-processing, even in areas where the fringes density is high. Right frames of both figures show examples in which the identification of fringes in areas with high fringes remains difficult (see black ellipses).

4. PROCESSING: ESTIMATION OF VIBRATION AMPLITUDES

4.1. Overview

The processing method we propose for estimating the qualitative map of vibration amplitudes from PSTA shearography measurements is based on a correct outlining of the fringes in the original acquisition. To limit the corruptions due to the noise, we apply this method to the pre-processed image ($\Delta\phi_p$).

The method is based on the fact that the function of phase differences takes value 0 or π according to the sign of the Bessel function J_0 when the function $\overline{\delta_A}$ increases (see Fig. 2). Inside any fringe of $\Delta\phi_p$, the values of $\overline{\delta_A}$ vary between two zeros ξ_k, ξ_{k+1} of J_0. In first approximation, we assume that $\overline{\delta_A}$ is constant inside any fringe of $\Delta\phi_p$, i.e., $\overline{\delta_A}$ is a piecewise constant function with sub-domains corresponding to the regions in which $\Delta\phi$ takes the same constant value (0 or π), i.e. in which $\Delta\phi_p$ takes the value π/2 or 3π/2.

We obtain the sub-domains of $\overline{\delta_A}$ by segmenting $\Delta\phi_p$ into the regions on which it is constant (π/2 or 3π/2). Then, we build the function $\overline{\delta_A}$ by assigning a value to each of its sub-domains. The value is zero in the regions of zero-crossing (corresponding to vibration nodes), and is a zero-value of the function J_0 in the other regions.

There is insufficient information in the function $\overline{\delta_A}$ for directly estimating the function of vibration amplitudes φ_A. However, we can compute φ_A by integrating the function δ_A along the shear displacement,

$$\varphi_A = \int \delta_A \, \Delta_s \, ds\,, \;\; \delta_A = \overline{\delta_A}\,\mathrm{sign}(\delta_A). \tag{22}$$

The only missing information is the signs of δ_A. We estimate them in two steps. We first identify the regions of zero-crossing of δ_A, then we estimate the signs of the displacements according to the number of regions of zero-crossing. One region of zero-crossing is a priori known: the clamped part of the blade that does not undergo relative movement with respect to other part of the blade during the vibration. Therefore, we always assume that the vibration amplitude is zero at the clamping. If this region is the only region of zero-crossing, the sign of δ_A is constant in the other regions. We fix it at 1. Otherwise, we assume that it alternates between the values -1 and 1 on both sides of the regions of zero-crossing.

We can exploit information both in the function $\Delta\phi_p$ of phase differences and in the image I_m re-defined as

$$I_m = I_m J_0(\delta_A) \tag{23}$$

to automatically detect the regions of zero-crossing. Indeed, the fact that the Bessel function J_0 is maximum at 0 (see Fig. 2) implies that the function I_m is maximum when δ_A is zero. Moreover, since I_m multiplies the sinusoidal functions in Eq. (4), the computation of ϕ from Eq. (6) makes the signal-to-noise ratio of $\Delta\phi = \phi - \phi_r$ maximum. In conclusion, we can use the fact that the function I_m and the signal-to-noise ratio of $\Delta\phi$ are maximum in regions of zero-crossing to detect them. In the remainder of the paper, we also call the newly defined I_m the modulation intensity image. Its computation from the four acquisitions obtained for the phase-shifting technique derives directly from Eq. (4):

$$I_m = \frac{1}{2}[(I_3 - I_1)^2 + (I_0 - I_2)^2]^{1/2}. \tag{24}$$

Finally, we obtain the function φ_A by integrating δ_A along the shear displacement. Integrating a piecewise constant function provides a piecewise linear function. If this visual aspect prevents the good interpretation of the results, the method can improve it using mean-filtering. The resulting image is denoted $\varphi_{A,s}$.

In a future work, such post-processing could be avoided by looking rather for a solution where δ_A is more regular than a piecewise constant function, e.g., by assigning values interpolated between the zeros of the zero-th order Bessel function of first kind to the fringes of the pre-processed image.

4.2. Processing steps

Fig. 7 shows the block diagram of the processing stage. The method requires the definition of the blade through a mask M_b taking values 1 inside the blade and 0 in the background. Parameters a_m, p_e, T_m, δ_s, and s_f are introduced in the following sections.

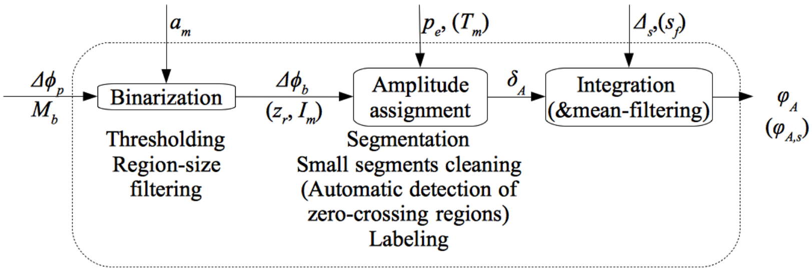

Fig. 7 Block diagram of the processing stage. Optional steps and their parameters are indicated in parenthesis.

4.2.2 Binarization

The binarization delineates the fringes of the denoised phase $\Delta\phi_p$ (obtained by pre-processing) and cleans the regions of too small size. It provides a binarized image $\Delta\phi_b$ and requires the minimum area of the regions (a_m) as parameter. The binarization is divided into two steps: the thresholding and the region-size filtering.

Thresholding. We convert $\Delta\phi_p$ into a binary image $\Delta\phi_b$ by setting the pixel values equal to 1 if original values are larger than π and to 0 otherwise. We assume that the segments with value 1 correspond to fringes of $\Delta\phi_p$ for which the phase difference is 3π/2, and that the segments with value 0 correspond to fringes of $\Delta\phi_p$ for which phase difference is π/2.

Region-size filtering. We remove regions with a size smaller than a percentage am of the area of the largest fringe (e.g., regions due to noise residuals). If the pixel intensities inside a region to suppress are equal to 1, they are set to 0, and vice versa.

4.2.2 Amplitude assignment

The amplitude assignment builds the function δ_A by assigning a value to each region of $\Delta\phi_b$. It is divided into the following steps: segmentation, small segments cleaning, possible automatic detection of zero-crossing regions, and labeling.

Segmentation. The segmentation divides the region defined by the blade mask into segments corresponding to the regions where $\Delta\phi_b$is constant. The algorithm applied for delineating the segments boundaries is the Moore-Neighbor tracing algorithm using the Jacob's stopping criterion [26]. The stages small-segments cleaning and labeling exploit the adjacency between segments. To make it possible, the segmentation also provides a table of adjacency strengths. We define the adjacency strength s_{kl} between two segments S_k, S_l as the number of pairs of pixels (p_k, p_l) such that p_k belongs to S_k, p_l belongs to S_l and p_k is adjacent to p_l. With this definition, the adjacency strength between two non-adjacent segments is equal to 0. For a segmentation of N segments, we define the table of adjacency strengths as the table A of N^2 elements, with element $A(k,l)$ defined as

$$A(k,l) = \frac{s_{kl}}{\sum_l s_{kl}}, \quad k,l = 0,\dots,N-1. \tag{25}$$

Small segments cleaning. The small-segments cleaning removes small holes caused by residual noise in the image Δϕp. Let us consider a segment S_k included in another segment S_l. This segment is small in comparison to S_k if its strength is smaller than 10% of the maximum strength among all strengths of segments adjacent to S_l. The adjacency table is used to locate such couples of segments (S_k, S_l). Indices k are the ones for which the row $A(k,.)$ has only one non-zero value. For each such index k, the index l is the one of the non-zero element $A(k,l)$. The adjacency table is also used to determine the strengths involved in the smallness condition.

Automatic detection of zero-crossing regions. The automatic detection of regions of zero-crossing is based on the fact that the function I_m (see equations (23) and (24)) and the signal-to-noise ratio of z are maximum in regions of zero-crossing. We indicate by $I_{m,p}$ the piecewise approximation of I_m, obtained by assigning the mean value of I_m to each segment of the segmentation. We indicate by n_z the number of regions of zero-crossing and by Z_k the regions of zero-crossing, with k in {0, 1, …, n_{z-1}}. Among these regions, we indicate by Z_0 the one that is a priori known: the region including the clamped part of the blade that is fixed during the vibration test. This zone can be easily identified by a point (parameter p_e).

The idea for identifying the regions Z_k is to find the regions Z that fulfill the two following conditions: (i) the standard deviation of z is higher on Z than on its adjacent regions, and (ii) the value of $I_{m,p}$ is higher on Z than on its adjacent regions. The noise contained in the image $I_{m,p}$ can lead to local maxima of $I_{m,p}$ generating artificial regions of zero-crossings. To prevent it, we replace in the second condition the image $I_{m,p}$ by its thresholded version $I_{m,T}$ using a threshold (parameter T_m):

$$I_{m,T} = \begin{cases} I_{m,p} \text{ if } I_{m,p} > T_m \\ 0 \text{ otherwise.} \end{cases} \tag{26}$$

Labeling. The labeling assumes that each region of zero-crossing has only one or two adjacent regions. Without this assumption, the information contained in images z and I_m is insufficient to estimate the sign of δ. The acquisitions should be conducted so that the produced measurements fulfill this assumption. This requires tuning the vibration frequency accordingly.

The labeling is performed in two steps: the estimation of $\overline{\delta_A}$ and the estimation of the signs of δ_A. The multiplication of the two resulting images provides an estimation of δ_A.

Estimation of $\overline{\delta_A}$ is made in two steps. First, we assign to each segment a null or positive integer n representing the order of succession of the region counted from the regions Z_k of zero-crossing. This step is iterative: it starts by assigning the value 0 to the regions Z_k, and then it operates iteratively using the adjacency table to process from each assigned region to its adjacent ones (by assigning the value $n + 1$ to each adjacent region of a region with n value). During the second step, we replace each n–value by the nth zero-value of the Bessel function J_0.

The estimation of the signs of δ_A is made in three steps. First, we merge the set of segments that are not the regions Z_k of zero-crossing. Let us indicate by n_m the number of obtained regions and by M_k the obtained regions, with k in {0, 1, …, n_{m-1}}. Then, we assign the sign 1 to the region M_k that is closest to the region Z_0 (the one including the clamped part). If there is more than one region of zero-crossing, there is also more than one region M_k and we assign to the other regions M_k the sign -1 or 1 by alternating between -1 and 1 on both sides of the regions Z_k.

4.2.3 Integration and mean filtering

Integration is achieved using the simplest inverse operator of the directional displacement operator, numerically approximated by finite differences. Let indicate by x the function resulting of the integration of a displacement image d along a vector δ_s of coordinates ($\delta_{s,1}$, $\delta_{s,2}$2) and of length $\overline{\delta_s}$. The value of x at any pixel p of coordinates (p_1, p_2) is computed from its value and the value of d at the pixel p' of coordinates ($p_1 - \delta_{s,1}$, $p_2 - \delta_{s,2}$):

$$x(p) = c(p) + x(p') + d(p'), \tag{27}$$

where function c is constant with respect to the integration direction. This latter function is initialized from the boundary conditions on the edges of the blade mask. The mean-filtering is a convolution with a square kernel of size s_f.

4.3. Results of processing

Different binary phase patterns obtained experimentally by PSTA shearography have been pre-processed and then processed, up to the integration to obtain amplitudes of vibratory displacement φ_A. The first example is the one of Mode 2 of Fig. 3 (left frame) which were pre-processed in Fig. 5. Fig. 8 show the subsequent processing steps for the two binary phase patterns corresponding to horizontal shear (top line) and diagonal shear (bottom line). Here the pre-processing for denoising is the TV technique. Figures (a) are the starting point of the processing displayed in Fig. 7. The results of binarization are shown in figures (b); the modulation images are shown in figures (c) and the latter are used to obtain the zero-crossing image shown in (d). Then the amplitude of phase difference δ_A are shown in figures (e). Finally the integration is performed to obtain the displacement amplitude map φ_A and is shown in figures (f).

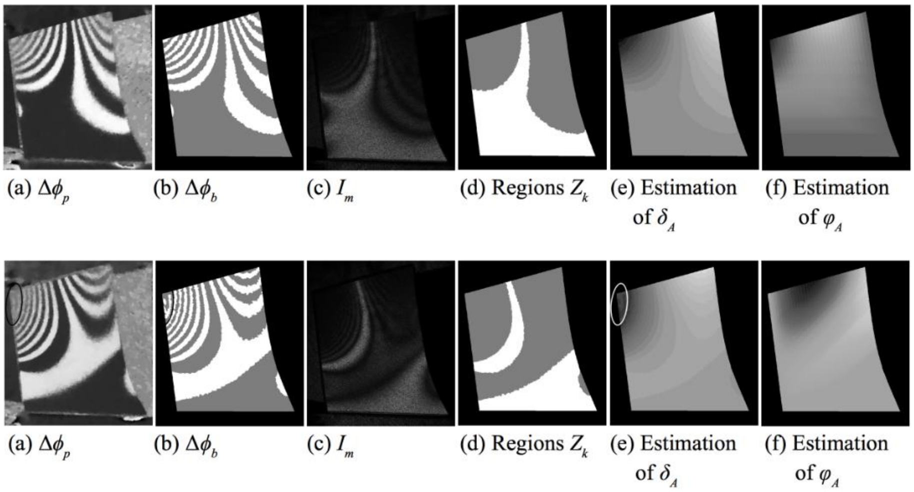

Fig. 8 Results of processed data for Mode 2 of Fig. 5 in the horizontal shear direction (top line) and diagonal shear direction (bottom line) after TV denoising.

Similar results are shown in Fig. 9 concerning patterns obtained by PSTA shearography in industrial environment. They correspond to the pre-processed data shown in Fig. 6. In this case, the top line pattern was denoised by TV and the one at the bottom line by MF. We see that, in the case of the bottom line, quality of fringes is not good on some parts of the pattern (black ellipse) and that it brings problem to the final results, both in δ_A and in the integration result φ_A.

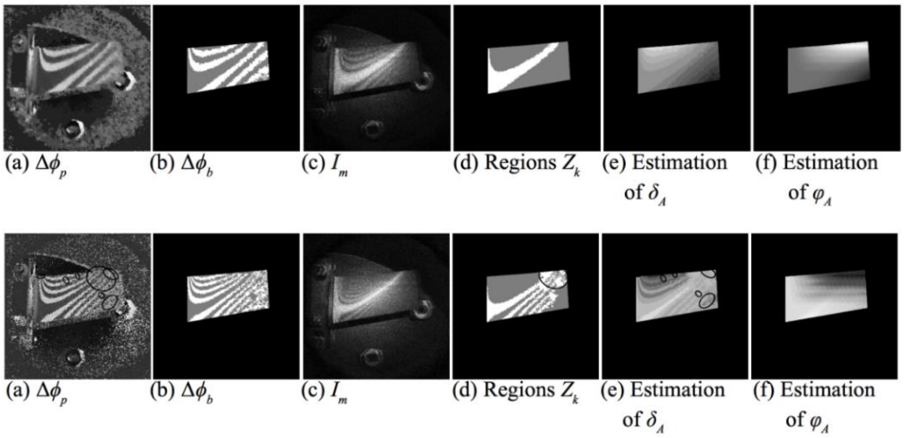

Fig. 9 Results of processed data for industrial data: (top line) images corresponds to Mode (f) of Fig. 3 (denoised by TV); (bottom line) images corresponds to Mode (g) of Fig. 3.

5. CONCLUSION

Shearography is a contactless optical technique used for vibration analysis. Non-experts in this field can easily interpret the vibration measurements if they have access to the maps of their amplitudes. However, shearography does not provide such maps but rather phase differences related to the derivative of displacements. Moreover, in our case we use a very simple methods based on phase-shifting applied in time-averaging mode (PSTA). This allows one to obtain rapidly patterns with correct quality in industrial environments. However, PSTA returns binary phase patterns. In this paper, we proposed a method for estimating the vibration amplitudes from shearographic measurements under the PSTA method, tackling the effect of different noise sources that are present in the experimental data The method is divided into two stages: pre-processing and processing. The main goal of the pre-processing is to reduce the noise contained in the shearographic acquisitions. We considered two denoising techniques. The processing stage, including spatial integration, provides a map of vibration amplitudes from a less noisy estimation of the initial image (the pre-processed image).

Experiments on synthetic data revealed that TV denoising outperforms MF denoising in terms of noise reduction, especially for large fringes densities. Experiments on real data acquired show that, for almost all acquisitions, the noise level and the fringes density are in an adequate range for delivering images of vibration amplitudes of good quality suitable for interpretation by non-experts. In addition, experiments on data acquired in optics laboratory show the adequacy of the proposed method for identifying vibration modes.

6. ACKNOWLEDGMENTS

The study presented in this paper has been achieved in the AOC project, funded by Wallonia DG06 (contract 6894), and through Belgian F.R.S.-FNRS grant.

REFERENCES

[1] Kreis, T., [Holographic Interferometry], Wiley-VCH Verlag GmbH & Co. KGaA, (2005).

[2] Steinchen, W., and Yang, L., [Digital Shearography: Theory and Application of Digital Speckle Pattern Shearing Interferometry], SPIE Press (2003).

[3] Kalms, M. K., and Osten, W., "Mobile shearography system for the inspection of aircraft and automotive components,"" Opt. Eng. 42(5), 1188–1196 (2003).

[4] Francis, D., Tatam, R. P., and Groves, R. M., "Shearography technology and applications: a review," Meas. Sci. Technol., 21(10), 102001 (2010).

[5] Creath, K., Slettemoen, G. Å., "Vibration-observation techniques for digital speckle-pattern interferometry," J. Opt. Soc. Am. A 2(10), 1629–1636 (1985).

[6] Vikhagen, E., "Vibration measurement using phase shifting TV-holography and digital image processing," Opt. Comm 69(3), 214–218 (1989).

[7] Yang, L., Steinchen, W., Kupfer, G., Mäckel, P., Vössing, F., "Vibration analysis by means of digital shearography," Opt. Lasers Eng. 30 (2), 199–212 (1998).

[8] Nakadate, S., Saito, H., Nakajima, T., "Vibration Measurement Using Phase-shifting Stroboscopic Holographic Interferometry," Opt. Acta Int. J. Opt. 33(10), 1295–1309 (1986).

[9] Borza, D. N., "Full-field vibration amplitude recovery from high-resolution time-averaged speckle interferograms and digital holograms by regional inverting of the Bessel function," Opt. Lasers Eng. 44(8), 747–770 (2006).

[10] Borza, D. N., "High-resolution time-average electronic holography for vibration measurement," Opt. Lasers Eng. 41(3), 515-527 (2004).

[11] Borza, D. N., "A new interferometric method for vibration measurement by electronic holography," Exp. Mech. 42 (4), 432–438 (2002).

[12] Vandenrijt, J.-F., Thizy, C., Georges, M. P., "Vibration analysis by speckle interferometry with CO2 lasers and microbolometers arrays," in Imaging and Applied Optics 2014, DTh4B.8. (2014).

[13] Languy, F., Vandenrijt, J-F., Thizy, C., Rochet, J., Loffet, C., Simon, D., Georges, M.P.., "Vibration mode shapes visualization in industrial environment by real-time time-averaged phase-stepped electronic speckle pattern interferometry at 10.6 µm and shearography at 532 nm," Opt. Eng. 55 (12), 121704–121704 (2016).

[14] Creath, K., "Phase-Measurement Interferometry Techniques," Prog. Opt. 26, 349–393 (1988).

[15] Rudin, L. I., Osher, S., Fatemi, E., "Nonlinear total variation based noise removal algorithms," Phys. Nonlinear Phenom. 60 (1), 259–268 (1992).

[16] Aebischer, H., Waldner, S., "Simple and effective method for filtering speckle-interferometric phase fringe patterns," Opt. Comm, 162(4), 205-210 (1999).

[17] Pitas I., Venetsanopoulos, A. N., [Nonlinear Digital Filters: Principles and Application]. Kluwer Academic Publisher, (1990).

[18] Bovik, A. C., Huang, T. S., Munson, J. D. C., "The Effect of Median Filtering on Edge Estimation and Detection," IEEE Trans Pattern Anal Mach Intell. 9(2), 181–194 (1987).

[19] Nikolova, M., "A Variational Approach to Remove Outliers and Impulse Noise," J. Math. Imaging Vis. 20(1), 99–120 (2004).

[20] Chambolle, A., Pock, T., "A First-Order Primal-Dual Algorithm for Convex Problems with Applications to Imaging," J. Math. Imaging Vis. 40(1), 120–145 (2011).

[21] Starck, J-L., Candes, E. J., Donoho, D. L., "The curvelet transform for image denoising," IEEE Trans. Image Process. 11(6), 670–684 (2002).

[22] Bergmann, R., Laus, F., Steidl, G., Weinmann, A., "Second Order Differences of Cyclic Data and Applications in Variational Denoising," SIAM J. Imaging Sci. 7(4), 2916–2953 (2014).

[23] Parikh, N., Boyd, S., "Proximal Algorithms," Found Trends Optim, 1 (3), 127–239 (2014).

[24] Sachs, L., [Applied statistics: a handbook of techniques], 2nd ed. New York, NY: Springer-Verlag, (1984).

[25] Gonzalez, R. C., Woods, R.E., Eddins, S. L., [Digital image processing using MATLAB®]. Prentice Hall (2004).